ISSN 0018-151X, High Temperature, 2016, Vol. 54, No. 4, pp. 547–554. © Pleiades Publishing, Ltd., 2016.
Original Russian Text © V.A. Bashkin, I.V. Egorov, I.V. Ezhov, 2016, published in Teplofizika Vysokikh Temperatur, 2016, Vol. 54, No. 4, pp. 576–583.

HEAT AND MASS TRANSFER AND PHYSICAL GASDYNAMICS

Circular Cylinder in a Transonic Flow at High Reynolds Numbers: Thermal Problem

V. A. Bashkin, I. V. Egorov*, and I. V. Ezhov

Zhukovskii Central Aerohydrodynamic Institute, Zhukovskii, 140180 Russia

**e-mail: ivan.egorov@tsagi.ru*

Received June 19, 2014

Abstract—The results of numerical simulation of transonic cross flow of a perfect gas around a circular cylinder at high Reynolds numbers are used to solve the thermal problem. The temperature distributions along the central line and the influence of Reynolds and Mach numbers on them are presented. The temperature fields and the transition of the near-wake solution to the far-wake solution are studied.

DOI: 10.1134/S0018151X16040040

INTRODUCTION

The computational aerodynamics methods are widely applied to obtain the comprehensive information about the flow of a viscous perfect gas around bodies of various configuration. In particular, the results of parametric calculations of transonic cross flow of a viscous perfect gas around a circular cylinder at high Reynolds numbers were presented and discussed in [1–9]. The main attention in these studies was paid to the dynamic problem, and only occasionally were some questions of the thermal problem considered.

During transonic flow around a blunt body with a heat-insulated surface, the maximum temperature in the flow field changes in a relatively narrow range. For example, the stagnation temperature of the incoming flow is determined by the formula $T_o = T_o/T_\infty = 1 + 0.5(\gamma - 1)M_\infty^2$, where γ is the adiabatic index and T_o and T_∞ are, respectively, the stagnation and static temperatures of the incoming flow. In the range of Mach numbers under consideration, $M_\infty = 0.8–1.3$, and the stagnation temperature changes only slightly (T_o = 1.13–1.34).

Nevertheless, the velocity and temperature fields interact intensively, which may induce interesting phenomena. For example, a significant thermal-energy redistribution in the near wake behind a circular cylinder was found experimentally in [10], due to which vortices in the Karman vortex trail have a "cold" nucleus and "hot" external layers (Eckert–Weise effect). This effect at transonic velocities was studied in [11].

Although the temperature in the flow field changes only slightly, it affects, due to compressibility of the moving medium, the distribution of the gas-dynamic variables (especially in the near wake and near-wall boundary layers because of high temperature gradients). This factor can change the flow-field structure. Therefore, the solution of the thermal problem and the influence of the gasdynamic similarity parameters on it are of scientific and practical interest.

In this paper, we report the results of studying the thermal-problem solution for a circular cylinder in a transonic perfect-gas flow at high Reynolds numbers.

1. STATEMENT OF THE PROBLEM AND NUMERICAL SIMULATION

The statement of the problem and numerical simulation, based on the Navier–Stokes equations (laminar flow) and the Reynolds equations (laminar-turbulent flow), of the transonic cross flow of a perfect gas around a circular cylinder were described in detail in [5, 6]; therefore, only brief comments on these questions are given below.

To integrate numerically the determining system of equations, we pass to the dimensionless variables according to the formulas

$$x^* = xR,\ y^* = yR,\ z^* = zR,\ u^* = uV_\infty,\ v^* = vV_\infty,$$
$$w^* = wV_\infty,\ p^* = p\rho_\infty V_\infty^2,\ t^* = tR/V_\infty;$$

the other gasdynamic variables correspond to their values in the incoming flow. Here, asterisks indicate the current dimensional quantities.

It was assumed in the numerical simulation that the perfect gas obeys the Clapeyron state equation and has a constant specific heat with adiabatic index $\gamma = 1.4$, Prandtl number Pr = 0.7, and a dynamic viscosity coefficient, which depends on the temperature according to the power law, $\mu \sim T^\omega$ ($\omega = 0.76$).

When carrying out the main series of calculations, the gas-dynamic similarity parameters (Reynolds and Mach numbers) were varied in the following ranges: $10^3 \le Re \le 10^6$ (laminar flow) or $10^6 \le Re \le 10^7$ (turbu-

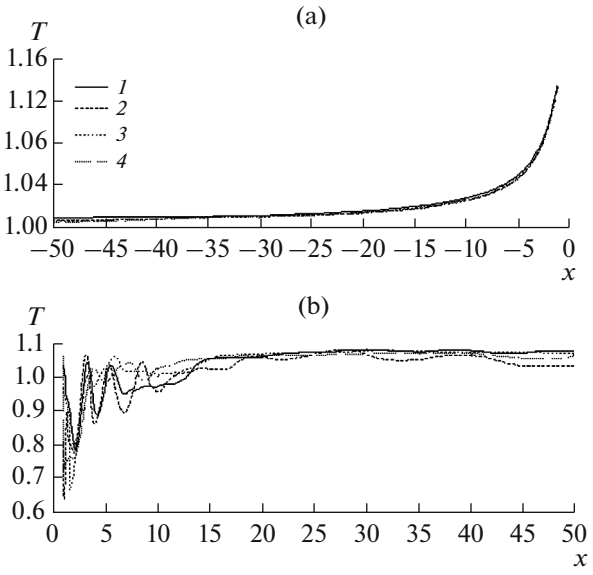

Fig. 1. Temperature distribution $T = T/T_\infty$ along the abscissa axis (a) before and (b) behind the heat-insulated cylinder for different Reynolds numbers at $M_\infty = 0.8$ and $t = 200$ (turbulent flow): (*1*) $Re = 10^3$, (*2*) 10^6, (*3*) 10^5 and (*4*) 10^7; (*1*, *2*) laminar regime, (*3*, *4*) turbulent regime.

lent flow) and $0.8 \le M_\infty \le 1.3$; the flown cylinder surface was assumed to be heat-insulated ($[\partial T/\partial n]_w = 0$, absolutely heat-insulating wall). To analyze the influence of the temperature factor, we performed special calculations for the transonic flow around a circular cylinder with the isothermal surface in a limited range of variation in the gasdynamic similarity parameters $Re = 10^5$ and 10^6 and $M_\infty = 0.8–1.3$ for two temperature factor values ($T_{w0} = 0.5$ and 1.5, absolutely heat-conducting wall). For the specified motion conditions (M_∞, Re), there are three problems with different temperature conditions at the flown surface.

The calculation data was obtained on an orthogonal nonuniform grid with 201 × 401 nodes, and the sizes of the calculation domain were 50 cylinder diameters in the horizontal direction (upstream and downstream) and 100 diameters in the vertical direction (upwards and downwards from the cylinder). To resolve the boundary layers near the solid surface, we selected three regions with thicknesses of $1/Re$, $2/Re^{1/2}$, and $1.5/Re^{1/5}$ containing, respectively, 6, 20, and 25% of the total number of nodes after crowding in the transverse direction. It should be noted that the blocking coefficient for the aforementioned calculation conditions is $k = 2R/200R = 0.01$, which is smaller than the limiting value ($k_{lim} \approx 0.05$ [12]); therefore, it does not affect the numerical-simulation results.

The governing equations were numerically integrated in the time interval $0 \le t = t^* V_\infty / R \le 200$ with a constant step $\Delta t = 0.01$, and the fields of the gasdynamic variables were recorded with a period $\delta t = 0.1$. According to the numerical experiments, when obtaining the stationary solution, the establishment of the general and "fine" flow-field structures takes the times $t \le 100$ and $t \le 150$, respectively. Thus, the chosen time interval is quite sufficient for the problem solution to achieve the quasi-periodic flow mode.

2. TEMPERATURE DISTRIBUTION ALONG THE CENTRAL LINE

The flow-field properties are determined by analyzing the fields of gasdynamic variables, which are subdivided into elementary (pressure, density, temperature, and velocity vector components) and complex (vorticity, heat flux, etc.). The problem under study includes a quite large number of the fields of gasdynamic variables. In [1–9], attention was paid primarily to the solution of the dynamic problem (in particular, the vorticity behavior in the near and far wakes). The solution of the thermal problem, described by the energy equation, will be analyzed below. The numerical solution is referred to as the main basic solution in the flight regime ($M_\infty = 0.8$, $Re = 10^3$) and the basic solution in the regimes with $M_\infty = 0.8$ and $Re \ne 10^3$.

The quality of the numerical simulation is often estimated from the distributions of gasdynamic variables along the abscissa axis before the cylinder. The plotted distributions of the pressure coefficient, temperature, Mach number, and longitudinal and normal velocity-vector components exhibit a monotonic behavior and an asymptotic achievement of a specified value at $x \to -\infty$. Each distribution barely depends on the Re number and flow regime and can be considered as a universal dependence. For example, Fig. 1a shows the temperature distributions for the basic solutions ($M_\infty = 0.8$; laminar and turbulent flow regimes).

This behavior of the gasdynamic variables on the abscissa axis also indicates the stationarity of the flow in this region: nonstationary processes occurring in the stern region and midsection of the cylinder cannot pass to the flow region in the vicinity of the front critical point. While moving away from it, nonstationarity effects become more intense and, upon reaching the midsection, manifest themselves to the full extent.

There are the near- and far-wake regions downstream behind the cylinder (in the vicinity of the flown body and at the output boundary of the calculation region, respectively). The solution of the problem for these regions determines the character of flow in the near and far wakes. To establish the flow character, we consider the temperature distribution in the basic solutions along the abscissa axis behind the body around which the flow moves (Fig. 1b).

According to the reported data, the flow is nonstationary in the near wake and the temperature fluctua-

tions have rather high amplitude (the time-averaged temperature is below unity).

It can also be seen in Fig. 1b that the viscous-gas temperature in the near wake reaches the far-wake mode with a relatively high speed: at $x \approx 15$ it possesses close-to-constant values, and at $x > 15$ the "fine" far-wake structure is established. It is a "three-layer sandwich" (Eckert–Weise effect), containing a "cold" nucleus (central part) and "hot" peripheral regions. Achievement of the far-wake solution will be discussed below in Section 5.

The wake behind the flown body is generally divided into three regions: near wake, transition region (wake "neck"), and far wake. Since each region is smoothly transformed into another, their boundaries are relative and depend on the chosen basic material. A two-region wake model with the near wake at $\approx x \le 18$ and far wake at $x \ge 18$ is well-substantiated for the considered temperature distributions of the basic solutions. This model is in good agreement with the two-region model for an incompressible liquid, which can be obtained by replacing the constant "18" with the constant "20" (see, for example, [13]).

Let us consider the influence of the Mach number on the temperature distribution along the central line by the example of the main basic solution (Fig. 2). A change in the number M_∞ modifies the temperature distribution behind and before the body. The dependences obtained before the cylinder have a smooth form, which indicates that the flow at the windward cylinder side is stationary with a maximum temperature at the front critical point.

Behind the cylinder around which the flow moves, the increase in the Mach number causes a deformation of the temperature distribution, resulting in two groups of curves with different forms corresponding to different regimes of flow around the cylinder. The first group consists of the temperature distributions for the numbers $M_\infty = 0.8$ and 0.9, corresponding to the first (subsonic) regime of flow around the cylinder. For all the other numbers M_∞ (when the second (supersonic) flow regime is implemented), the corresponding dependences comprise the second group of temperature distributions with a form similar to that for solution of the stationary problem.

The calculations showed that a change in the Mach number at a fixed number Re affects significantly the temperature distribution along the central line in the case of adiabatic flow around the circular cylinder. At the same time, one often deals with nonadiabatic flow in practice (for example, flow around thermal elements in heat-exchangers); the most widespread case is an isothermal surface around which the flow moves. Special calculations were performed to determine the influence of the isothermal surface on the temperature field; the calculated temperature data used in the comparative analysis are shown in Fig. 3.

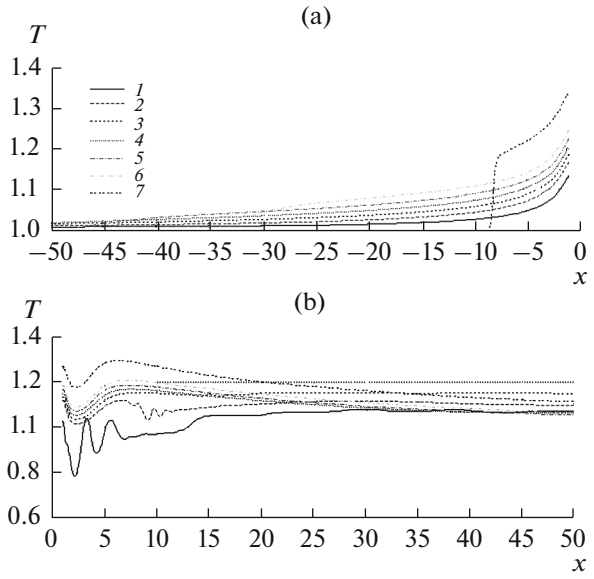

Fig. 2. Temperature distribution $T = T/T_\infty$ along the abscissa axis (a) before and (b) behind the heat-insulated cylinder for different Mach numbers at $Re = 10^3$ and $t = 200$: (*1*) $M_\infty = 0.8$, (*2*) 0.9, (*3*) 0.95, (*4*) 1.00, (*5*) 1.05, (*6*) 1.10, and (*7*) 1.30.

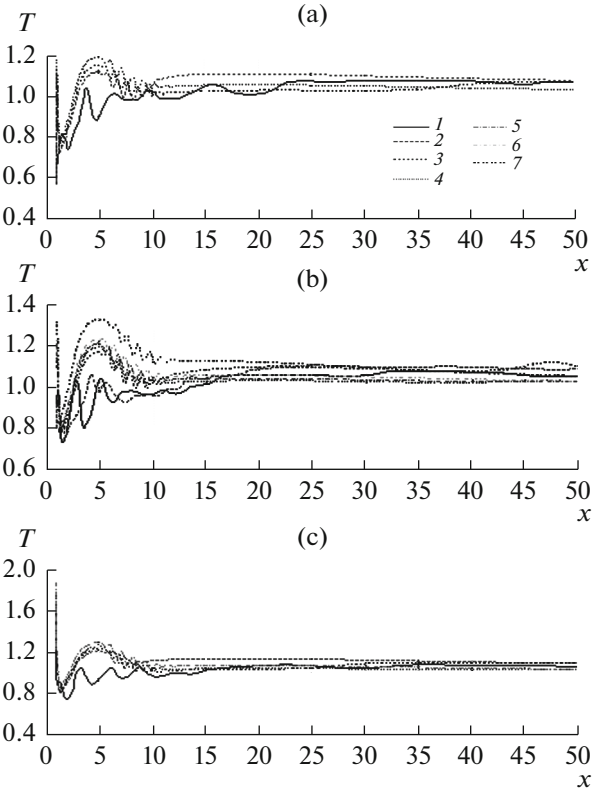

Fig. 3. Temperature distribution $T = T/T_\infty$ along the central line behind the circular cylinders with different thermal conditions at the flown surface for different Mach numbers at $Re = 10^5$ (laminar flow): (a) $T_{wo} = 0.5$, (b) $\partial T/\partial n = 0$, and (c) $T_{wo} = 1.5$; the designations of the curves are the same as in Fig. 2.

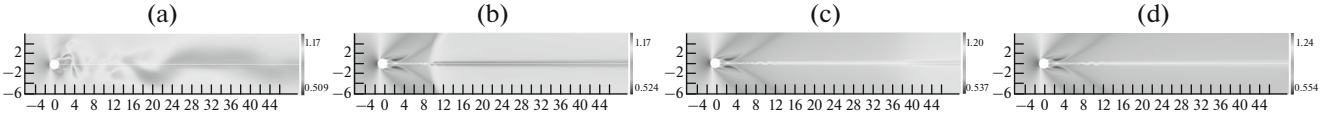

Fig. 4. Patterns of the temperature fields $T = T/T_\infty$ near the isothermal ($T_{wo} = 0.5$) cylinder at $\mathrm{Re} = 10^5$ and $t = 200$: (a) $\mathrm{M}_\infty = 0.8$, (b) 0.9, (c) 1, and (d) 1.1.

The temperature distributions in the wake are consistent with the two-region model, and the calculation results show that the largest temperature differences are observed in the near wake; the calculated dependences for the far wake are located compactly, in a narrow band.

As was noted above, the temperature distributions for the heat-insulated cylinder are divided into two groups (according to the shape of the curves), corresponding to different cylinder-flow regimes. In this specific case, the second group is subdivided into two subgroups of curves with similar shapes but different degrees of instability in the portion behind the maximum temperature. In both cases, the transition to the isothermal cylinder leads to a denser position of the curves; the densest pack of the curves is obtained for the superheated surface.

3. TEMPERATURE FIELDS

The temperature distributions along the central line indicate the complex character of the temperature field and the dependence of its structure on the governing parameters of the problem.

As an example, we consider the influence of the Mach number on the temperature field around the circular cylinder with an isothermal ($T_{wo} = 0.5$, moderate heat transfer) surface at the fixed number $\mathrm{Re} = 10^5$ (Fig. 4).

At $\mathrm{M}_\infty = 0.8$ (as one would expect), we have nonstationary flow around the cylinder (near wake) and the nonstationary flow in the far wake (Fig. 4a). The temperature field clearly shows the flow regions with different temperature conditions; the supersonic region formed in the near wake is an interesting mosaic pattern. When passing to the numbers $\mathrm{M}_\infty \geq 0.9$, the second (supersonic) flow regime is implemented and the temperature-field pattern changes. For $\mathrm{M}_\infty = 0.9$, a supersonic region of perturbed flow with the base $-1 \leq x \leq 10$ is formed near the cylinder (Fig. 4b). Behind it, there is a region of uniform subsonic stationary flow (on the whole, the pattern resembles the scheme of flow around a thin profile within the linear theory). Stagnation of the supersonic flow occurs through a complex system of compression shocks and compression and expansion waves; the final shock wave begins at the central line in the cross section $x \approx 10$ and degenerates into the Mach line as it moves away from the central line. The temperature-field structure can be established only partially from the direct images; additional useful information about the near-wake structure can be obtained from the inverted images. In this context, we should note that the main purpose of this study is an analysis of the temperature behavior in the wake behind the circular cylinder in the transonic flow; therefore, specific features of the flow in the external field are not considered in detail and are mentioned only in passing.

At the unit Mach number, the pattern changes again (Fig. 4c): the base of the perturbed flow region narrows ($1 \leq x \leq 5$), and the regions of variable ($5 \leq x \leq 38$) and constant ($38 \leq x \leq 50$) temperature successively occur downstream. During this transition, the gas-dynamic variables behave as follows: the pressure coefficient and the normal velocity-vector component gradually tend to zero, the longitudinal velocity component decreases from 0.9 to 0.8, and the temperature increases to about 1.05. This transition indicates the process of transformation of the supersonic flow into the subsonic one through the compression wave (according to the presented image, the transition flow is isoentropic). The pattern somewhat changes again at the number $\mathrm{M}_\infty = 1.1$ (Fig. 4d): the perturbed-flow region is followed by one region of constant temperature ($5 \leq x \leq 50$). These results are in agreement with the behavior of the gas-dynamic variables at the central wake line.

4. TEMPERATURE OSCILLATIONS AT THE CENTRAL WAKE LINE

The behavior of the dynamic-problem solution near the transition from the near wake to the far wake was considered in [7]. The temperature behavior in the aforementioned wake region will be analyzed below as applied to the main basic solution ($\mathrm{M}_\infty = 0.8$, $\mathrm{Re} = 10^3$).

Let us begin with a brief description of the evolutionary dependences for fixed points on the central wake line. Although they are not given here, their qualitative estimation clarifies specific features of the amplitude–frequency characteristic (AFC).

At the point $x = 10$, the dependence of the evolution is regular with pronounced periodicity and describes the process of transition to a new value of the oscillation axis (≈0.974). It exhibits irregular behavior at the point $x = 20$ and oscillates in a complex way around the constant value of ≈1.057. At the point $x = 30$, the dependence of the evolution oscillates regularly around the constant of ≈1.074. At the two subsequent

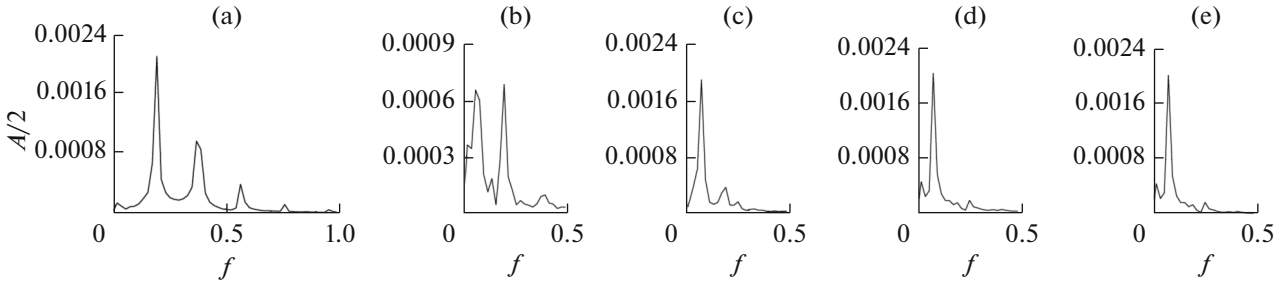

Fig. 5. AFC of the temperature T at a fixed point of the flow field near the heat-insulated circular cylinder in the transonic flow ($M_\infty = 0.8$ and $Re = 10^3$, laminar flow): (a) $x = 10$, (b) 20, (c) 30, (d) 40, and (e) 50.

points, the oscillations occur in the output region of the calculation domain around the constants of 1.078 and 1.068. Note that the output flow regime is retained during the last 100 units of dimensionless time for all five fixed points.

Now let us investigate the AFC of the oscillating temperature at fixed points of the wake. Having applied the Fourier analysis to the corresponding evolutionary dependence, we obtain the AFC for a fixed point under consideration at the central wake line (Fig. 5); the processed calculation results are printed out as plots and tables. The program formally processes all the points with a local temperature maximum; however, they have close values and are determined with a low accuracy in the region of high-frequency oscillations. At the point $x = 10$, the AFC is a discrete spectrum with three dominant frequencies (Fig. 5a); its intensity decreases with an increase in frequency: (Sh_T, A/2) = (2F, A/2) ≈ (0.390625, 0.002098), (0.742187, 0.0009651), and (1.132817, 0.0003885). In other words, there are three levels of Strouhal numbers at the flow-field point $x = 10$.

The oscillating-temperature AFC is a continuous narrow-band spectrum at the point $x = 20$ (Fig. 5b) and indicates the existence of two dominant frequencies (two-level solution) with roughly identical intensities (Sh_T, A/2) = (2F, A/2) ≈ (0.390625, 0.0006832) and (0.117187, 0.0006529). For the three subsequent points, the AFCs coincide (Figs. 5c–5e) and correspond to one dominant frequency (Sh_T, A/2) = (2F, A/2) ≈ (0.15625, 0.0021) (single-level solution).

Figure 6 shows the distribution of the Strouhal number along the central wake line, as well as the distribution of the averaged temperature, which changes slightly along the central wake line tending to an asymptotic value from above. This fact does not contradict the known calculation results and indicates the reliability of the information obtained from the numerical simulation.

The first-level Strouhal number in the range $20 < x < 30$ is likely to have a discontinuity at the transition to a smaller value; the first-level distribution $Sh_T = Sh_T(x)$ is a piecewise constant function with values consistent with the numbers Sh for the gas-dynamic variables in the near wake (therefore, the temperature oscillations are generated by the escape of vortices from the surface around which the flow moves). The second-level Strouhal numbers have values at the first two points that are not in agreement with the typical values for the gas-dynamic variables in the near wake. The situation for the third-level number Sh is similar.

5. TEMPERATURE MODE OF THE SURFACE AROUND WHICH THE FLOW MOVES

The temperature mode of the surface around which the flow moves is of some practical interest. In the case of adiabatic flow, the surface temperature is determined by solving the problem for the Mach and Reynolds numbers specified; for the isothermal cylinder, we have constant temperature of the surface set in the boundary conditions. Three problems with the following thermal boundary conditions at the cylinder surface were solved for each pair of the Mach and Reynolds numbers: (i) $\partial T/\partial n = 0$ (no heat transfer, adiabatic wall), (ii) $T_{wo} = \text{const} = 0.5$ (moderate heat transfer, cooled wall), and (iii) $T_{wo} = \text{const} = 1.5$ (moderate heat transfer, overheated wall). As was mentioned above, the selective calculations were per-

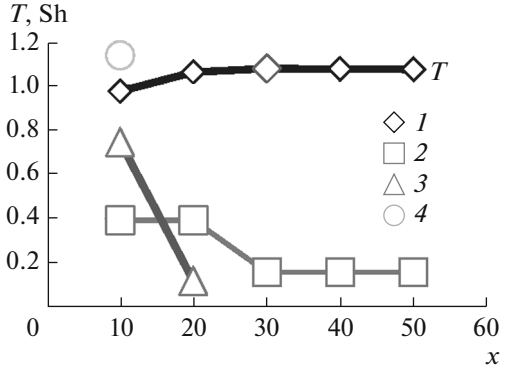

Fig. 6. Distribution of the average temperature $\langle T \rangle$ at the central wake line for the main basic solution and the Strouhal numbers of different levels: (*1*) average temperature $\langle T \rangle$, (*2*) first level, (*3*) second level, and (*4*) third level.

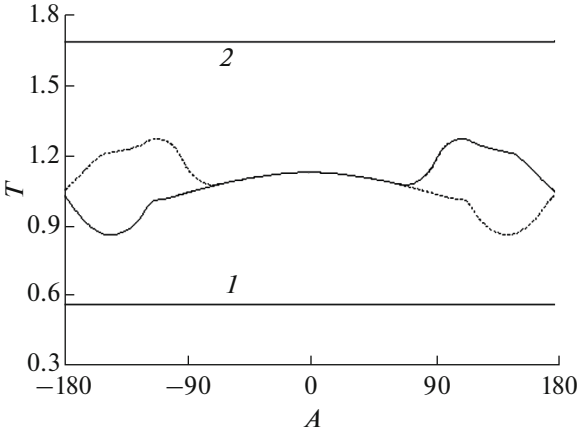

Fig. 7. Temperature mode of the flown surface of the circular cylinder in the transonic flow: $0^+ \le \theta \le 180°$ for the upper side and $0^- \ge \theta \ge -180°$ for the lower side; the solid and dashed lines indicate the first and second basic state, respectively; (*1*) $T_{wo} = 0.5$ ($T_{w\infty} = 0.564$, cooled surface) and (*2*) $T_{wo} = 1.5$ ($T_{w\infty} = 1.692$, overheated surface).

formed in a limited range of variation in the governing similarity parameters.

As an example, Fig. 7 shows the results of calculating the temperature of the cylinder surface for the numbers $M_\infty = 0.8$ and $Re = 10^3$ and the laminar flow regime.

The surface of the heat-insulated cylinder has a variable temperature, referred to as the restoration temperature $T_w(x, t) = T_R(x, t)$; therefore, Fig. 7 shows the calculated temperature distributions for two basic flow states: first and second, between which the temperature oscillates. The first (second) basic state corresponds to the case where the primary-detachment point occupies the extreme left position on the upper (lower) cylinder side. The straight-line dependences determine the temperature mode of the isothermal-surface cylinder for two different flow regimes.

It can be seen that the restoration-temperature distribution over the contour is nonuniform: a high, almost stationary temperature at the frontal surface and a low nonstationary temperature in the bottom region, which changes in a fairly wide range for the oscillation half-period. The highest nonuniformity in the temperature distribution is observed at the number $Re = 10^3$. An increase in the Reynolds number somewhat equalizes the temperature; however, the nonuniformity remains and approaches (in the region of flow without separation) the solution within the equations of the laminar boundary layer.

The maximum temperature at the adiabatic cylinder surface is at the front critical point and exceeds the stagnation temperature of the incoming flow $T_o = 1.128$. In addition, the absolute temperature maximum is observed in the vicinity of the primary-detachment point while approaching the basic state. This specific feature is due to the thermal-energy redistribution in the viscous gas flow, and the directionality of heat transfer is determined by the thermophysical properties of the moving medium (in particular, the Prandtl number, Pr).

Since there is a detachment zone at the bottom of the heat-insulated cylinder (where the flow velocities are small and the restoration temperature T_R is simultaneously the local stagnation temperature T_o), the "cold" region is formed in the near wake. This indicates a complex temperature-field structure, although the temperature in the transonic flow changes in a relatively narrow range.

The temperature profiles in different wake cross sections $x = \text{const}$ are plotted in Fig. 8 to illustrate the specific features of the temperature-field behavior. Figure 9 shows the isolines $\omega^* = \text{const}$ (dimensional vorticity), where cross sections $x = \text{const}$, corresponding to the plotted temperature profiles, are indicated. These profiles indicate the instantaneous state of the temperature field, which is determined to a large extent by the vorticity field, and demonstrate its development in the region of transition from the near wake to the far wake.

Near the cylinder (in particular, in the cross section $x = 1.48$), where the nonstationarity is weak and the

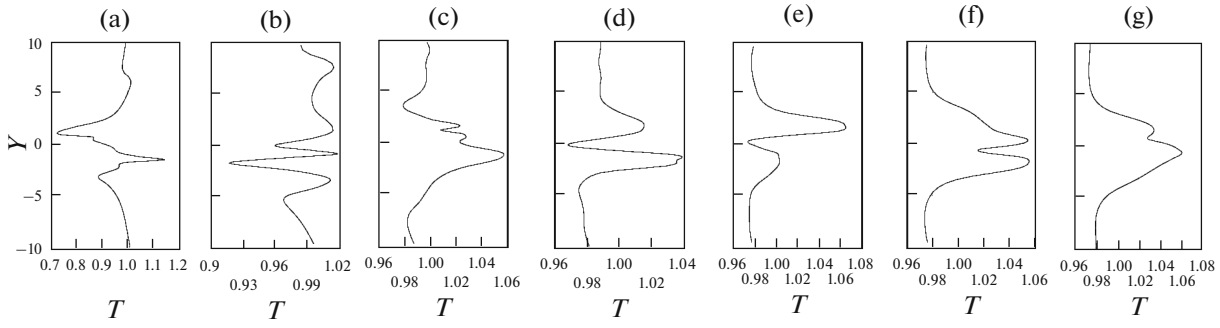

Fig. 8. Temperature profiles $T = T/T_\infty$ in the near wake of the circular heat-insulated cylinder in the transonic flow ($M_\infty = 0.8$, $Re = 10^3$, $t = 200$): (a) $x = 1.48$, (b) 2.88, (c) 5.78, (d) 8.76, (e) 11.68, (f) 14.71, and (g) 18.

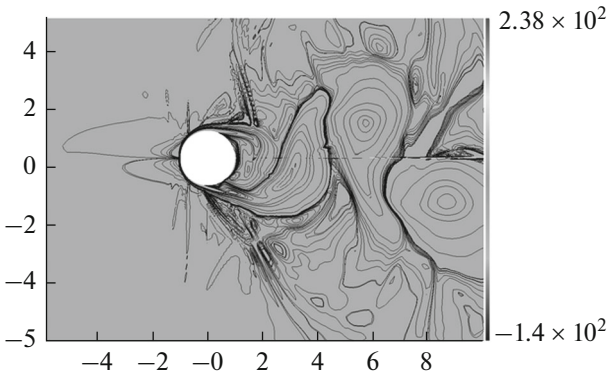

Fig. 9. Pattern of the vorticity isolines $\omega = L\omega^*/V_\infty = \text{const}$ (ω^* is the dimensional vorticity) in the near wake of the circular heat-insulated cylinder in the transonic flow with $M_\infty = 0.8$ and $Re = 10^3$.

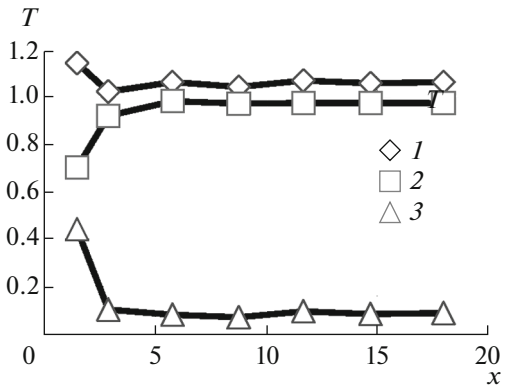

Fig. 10. Distribution of the characteristic temperatures along the central wake line behind the circular cylinder at $M_\infty = 0.8$ and $Re = 10^3$: (*1*) maximum temperature T_{max}, (*2*) minimum temperature T_{min}, and (*3*) temperature difference $\Delta = T_{max} - T_{min}$.

vorticity field is strongly nonuniform, the temperature profile in short (i.e., at $y \approx 0$) is an odd function, which is typical of the stationary solution of the problem. Downstream, the vorticity field becomes more uniform and the shape of the temperature profile is simplified (in short, it is either even ($x = 2.88$, 8.76, 11.68, and 14.71) or odd ($x = 1.48$, 5.78, and 18) function).

It was noted in Section 2, when analyzing the temperature distribution along the central wake line, that the far-wake structure is a "three-layer sandwich" ("cold" nucleus and "hot" periphery). The temperature profiles (Fig. 8) confirm the existence of the "three-layer sandwich" regions (there are several of them in the near wake). However, the interaction with the far-wake vortex structures reduces the intensity and increases the degree of nonuniformity of the vorticity; thus, it leads to fracturing of the "three-layer sandwich" while advancing downstream.

The temperature profiles are nonmonotonic and have several extrema, which allow one to analyze the development of the wake temperature mode. Figure 10 shows the distribution of the maximum (T_{max}) and minimum (T_{min}) temperatures along the central wake line and the temperature difference $\Delta = T_{max} - T_{min}$ in the wake cross section. The results for the profile in the cross section $x = 1.48$ are omitted here because they are not consistent with the profile data for the subsequent cross sections and determine the initial stage of near-wake formation. All the other temperature profiles correspond to the developed state of the near wake.

In the developed near wake, the extreme temperatures and their difference change only slightly along the central line; however, all these distributions indicate a stepwise change in their numerical values in the interval $9 < x < 11$. At the discontinuity, the minimum temperature slightly decreases, while the maximum temperature and the temperature difference somewhat increase. On the whole, this fact means the beginning of the interaction between the near- and far-wake vortex structures in this interval.

Figure 9 shows the isolines $\omega = \text{const}$ for the near wake and vortices of different scales according to the main basic solution. The multiscale vorticity leads to a strong nonuniformity of the temperature field in the wake region. The discussion of the vorticity isoline pattern is restricted to this brief comment, because this question was analyzed in detail in [7].

CONCLUSIONS

The thermal problem, described by the energy equation as applied to the circular cylinder, was discussed based on the calculation data obtained in a rather wide range of variation in the governing parameters of the problem. The the transonic stream of a viscous perfect gas at high Reynolds numbers flowed around the cylinder. The object of study was the temperature fields of the flow and their interaction with a body moving with a constant velocity.

On the windward side of the cylinder, the flow is almost stationary in the vicinity of the frontal stagnation point; however, while moving away from this point, nonstationary phenomena are enhanced, and they manifest themselves to the full extent beginning with the midsection (vortices periodically escape from the heat-insulated cylinder surface). The temperature distribution along the central line before the body has a maximum at the frontal stagnation point, decreases monotonically while moving away from it, and asymptotically tends to unity at $x \to -\infty$.

The flow is nonstationary on the leeward side of cylinder; the wake behind the cylinder satisfies the two-region model with respect to the temperature behavior: the near wake is at $\approx x \le 18$ and the far wake is at $\approx x \ge 18$. The onset point of interaction between

the near- and far-wake vortex structures is located in the calculation domain near the cylinder for the values of similarity parameters considered. Due to this, a "short" Karman vortex trail is formed behind the cylinder; a "long" Karman vortex trail is implemented at low Reynolds numbers ($Re < 10^3$).

At transonic velocities, the temperature in the perturbed-flow field changes in a narrow range; however, it affects significantly the flow field and the aerodynamic characteristics of the circular cylinder. For example, a change in the thermal boundary condition (replacement of the adiabatic surface with an isothermal one) changes the limiting Reynolds number Re* (a "fine" characteristic), at which the regime of flow around the cylinder changes.

The frequency characteristics of the oscillating temperature at the central wake line (the transition from the near wake to the far wake) were studied. In particular, it was shown that the average temperature changes only slightly while advancing downstream and the Strouhal number is a piecewise constant function.

ACKNOWLEDGMENTS

This study was supported by the Russian Science Foundation, project no. 14-19-00821.

REFERENCES

1. Bashkin, V.A., Egorov, I.V., Ezhov, I.V., and Ivanov, D.V., *Uch. Zap. Tsentr. Aerogidrodin. Inst.*, 2007, vol. 38, no. 3, p. 1.
2. Bashkin, V.A., Egorov, I.V., Ezhov, I.V., and Ivanov, D.V., *Uch. Zap. Tsentr. Aerogidrodin. Inst.*, 2007, vol. 38, no. 4, p. 1.
3. Bashkin, V.A. and Ezhov, I.V., *Uch. Zap. Tsentr. Aerogidrodin. Inst.*, 2011, vol. 42, no. 1, p. 12.
4. Bashkin, V.A., Egorov, I.V., Ezhov, I.V., and Utyuzhnikov, S.V., *Uch. Zap. Tsentr. Aerogidrodin. Inst.*, 2012, vol. 43, no. 5, p. 27.
5. Bashkin, V.A., Egorov, I.V., Ezhov, I.V., and Utyuzhnikov, S.V., *Uch. Zap. Tsentr. Aerogidrodin. Inst.*, 2013, vol. 44, no. 5, p. 3.
6. Bashkin, V.A. and Egorov, I.V., *Chislennoe modelirovanie dinamiki vyazkogo sovershennogo gaza (Numerical Simulation of the Dynamics of Viscous Perfect Gas)*, Moscow: Fizmatlit, 2012.
7. Bashkin, V.A. and Egorov, I.V., *Chislennoe issledovanie zadach vneshnei i vnutrennei aerodinamiki* (Numerical Studying of the Problems of Internal and External Aerodynamics), Moscow: Fizmatlit, 2013.
8. Egorov, I.V., Pal'chekovskaya, N.V., and Shvedchenko, V.V., *High Temp.*, 2015, vol. 53, no. 5, p. 677.
9. Bashkin, V.A., Egorov, I.V., and Pafnut'ev, V.V., *High. Temp.*, 2005, vol. 43, no. 5, p. 733.
10. Eckert, E.R.G. and Weise, W., *Forsch. Ingenieurwes.*, 1942, vol. 13, p. 246.
11. Rona, A. and Bennett, W.P., Energy separation in a compressible vortex street, *AIAA Paper* 2001–0601, 2001.
12. Anagnostopoulos, A., Iliadis, G., and Richardson, S., *Int. J. Numer. Methods Fluids*, 1966, vol. 22, no. 11, p. 1061.
13. Saha, A.K., *Phys. Fluids*, 2007, vol. 19, p. 128110.

Translated by A. Sin'kov